Available online at www.sciencedirect.com
ScienceDirect
Journal of Power Sources 159 (2006) 1422–1427
JOURNAL OF POWER SOURCES
www.elsevier.com/locate/jpowsour

Li diffusion in $LiCoO_2$ thin films prepared by pulsed laser deposition

Hui Xia [a], Li Lu [a,b,*], G. Ceder [a,c]

[a] *Advanced Materials for Micro- and Nano-System, Singapore-MIT Alliance, 4 Engineering Drive 3, 117576 Singapore*
[b] *Department of Mechanical Engineering, National University of Singapore, 9 Engineering Drive 1, 117576 Singapore*
[c] *Department of Materials Science and Engineering, Massachusetts Institute of Technology, Cambridge, MA 02139, USA*

Received 3 October 2005; received in revised form 10 December 2005; accepted 12 December 2005
Available online 2 February 2006

Abstract

Preferred *c*-axis oriented $LiCoO_2$ thin films were prepared on a Si substrate by pulsed laser deposition (PLD). The chemical diffusion coefficients, $\tilde{D}_{Li}$, of Li in these films were measured by electrochemical impedance spectroscopy (EIS) and potentiostatic intermittent titration technique (PITT). $\tilde{D}_{Li}$ was found to be in the range of 10^{-11} to 10^{-13} $cm^2\ s^{-1}$ depending on Li concentration and on the characterization method used.

Keywords: Thin-film battery; $LiCoO_2$; Lithium diffusion; Pulsed laser deposition

1. Introduction

$LiCoO_2$ is the most commonly used cathode material for rechargeable Li-ion batteries. Without the presence of a polymer binder and carbonaceous powders, the dense and flat thin films are ideally suited to study fundamental kinetic parameters such as lithium diffusivity.

The layered structure of $LiCoO_2$, a nearly cubic close-packed arrangement of oxygen ions with lithium and cobalt ions occupying alternate layers of octahedral sites, is well suitable for the rapid deintercalation and intercalation of lithium. When lithium is deintercalated or intercalated from or into the Li_xCoO_2 matrix, transformations of several phases occur as the lithium content, x, is varied between $x = 1$ and 0.5. These include a metal–insulator transition [1–3] and order–disorder reactions [4,5].

Lithium diffusion in the electrodes is a key factor that determines the rate at which a battery can be charged and discharged. With increasing interest in high power density, the kinetics of Li diffusion becomes more important. Many diffusion measurements on $LiCoO_2$ have been preformed on composite electrodes consisting of graphite, binders and other materials [6–9]. However, a detailed analysis of diffusion coefficients is difficult for composite electrodes because of their non-uniform potential distributions and unknown electrode surface area. As a result, published values for the chemical diffusion coefficient $\tilde{D}_{Li}$ vary over a wide range from 10^{-13} to 10^{-8} $cm^2\ s^{-1}$ [6–9]. Thin films with known composition and well-defined geometry may be more appropriate for diffusion measurements. Jang et al. [10] measured $\tilde{D}_{Li}$ in an all solid-state battery with a sputtered $LiCoO_2$ electrode. We have chosen a somewhat different approach using pulsed laser deposition (PLD) to obtain high quality dense $LiCoO_2$ film that can directly be measured in a cell with a liquid electrolyte. When testing thin film electrodes in liquid electrolytes, the quality and density of the electrode film is important because permeation of the electrolyte into cracks of the thin film can modify the surface area making it difficult to extract proper values of $\tilde{D}_{Li}$. PLD is, therefore, particularly well suited to making films for diffusion measurements. Striebel et al. [11], Julien et al. [12], Iriyama et al. [13] and Perkin et al. [14] have shown successful growth of $LiCoO_2$ with highly preferred (0 0 3) using PLD.

In this study, crack free $LiCoO_2$ thin films have been prepared by PLD. EIS and PITT were used to measure the chemical diffusion coefficients of lithium in $LiCoO_2$ thin films.

2. Experimental

2.1. Preparation of the $LiCoO_2$ thin film

$LiCoO_2$ thin films with buffer layers of Pt/Ti/SiO_2 were deposited on Si substrates by PLD where Pt was deposited as

* Corresponding author. Tel.: +65 6874 2236; fax: +65 6779 1459.
E-mail address: mpeluli@nus.edu.sg (L. Lu).

0378-7753/$ – see front matter © 2006 Elsevier B.V. All rights reserved.
doi:10.1016/j.jpowsour.2005.12.012

the current collector and a Ti buffer layer was used to increase adhesion between the Pt and SiO_2. Based on Julien et al. [12] the $LiCoO_2$ target was prepared with a 15% excess Li_2O to compensate for Li loss during deposition. The target and substrate were placed inside a vacuum chamber of the PLD which had a pressure of less than 1×10^{-5} Torr. The target–substrate distance was kept at 40 mm. During deposition, the target was rotated at 10–20 rpm to avoid depletion of material at any given spot. A Lambda Physik KrF excimer laser with wavelength 248 nm was used in the deposition. Laser fluence was controlled at 2 J cm^{-2} and a repetition rate at 10 Hz. Film deposition was carried out with 100 m Torr oxygen partial pressure at 600 °C for 40 min.

The deposited thin films were characterized by means of X-ray diffraction (XRD) with Cu Kα radiation and a scanning electron microscope (SEM). The thickness of the thin film was determined by SEM on a fractured cross-section of the sample.

2.2. Electrochemical characterization

All electrochemical experiments were conducted in an Ar-filled glove box using a Solartron 1287 two terminal cell test system combined with Solatron 1260 frequency response analyzer. Li-metal foil was used as both the anode and reference electrode. A $LiCoO_2$ thin film was used as the cathode. One mole $LiFP_6$ in a 1:1 (by volume) ethylene carbonate (EC)–diethylene carbonate (DEC) solution was used as the electrolyte. A beaker was adapted as the electrolyte container with both cathode and anode immersed in the beaker.

Galvanostatic charge–discharge was carried out in the potential range between 3.0 and 4.2 V with a constant current density of 15 μA cm^{-2}. The incremental capacity ($\Delta Q/\Delta V$) versus voltage, and the differential factor ($-dx/dV$) were derived from the charge–discharge curve. Electrochemical impedance spectra (EIS) were measured at various electrode potentials in the frequency range from 10 kHz to 3 mHz. The impedance data were analyzed by equivalent circuit fitting using ZView2 software of Scribner Company. To measure the chemical diffusion coefficient by potentiostatic intermittent titration technique (PITT), a potential step of 10 mV was applied and the current was measured as a function of time. The potential step was stepped to the next level while the current was below 0.1 μA cm^{-2}. This procedure was repeated between 3.89 and 4.20 V at both increasing and decreasing potentials.

3. Results and discussion

3.1. Characterization of $LiCoO_2$ thin films

Fig. 1 shows the XRD pattern of the $LiCoO_2$/Pt/Ti/SiO_2 on Si substrate. Three XRD peaks for $LiCoO_2$ at 2θ 18.98°, 38.46° and 59.25° can be seen, which are attributed to (0 0 3), (0 0 6) and (0 0 9) diffractions of rhombohedral $LiCoO_2$. Other diffraction peaks of $LiCoO_2$ such as (1 0 1), and (1 0 4) in this scan range could not be detected, indicating that the film had a preferred *c*-axis (0 0 3) out-of-plane orientation. The formation of preferred (0 0 *l*) orientation is attributed to (0 0 *l*) planes having the lowest surface energy no mattering using PLD or Sputtering method

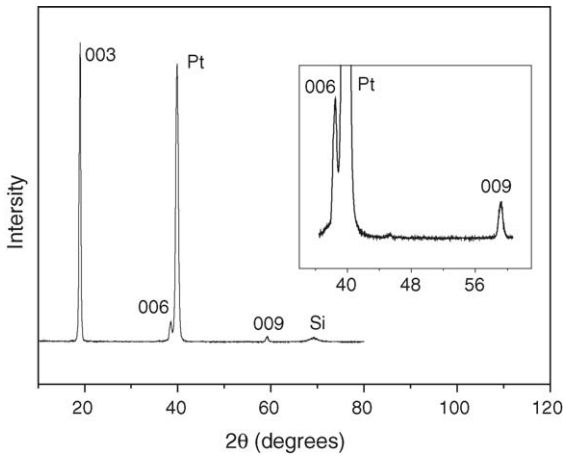

Fig. 1. XRD $\theta/2\theta$ spectrum for $LiCoO_2$ thin film on a Pt/Ti/SiO_2/Si substrate.

[13,15]. A very dense film without any pinholes and cracks was observed by SEM. The film thickness and deposition rate were estimated to be respectively about 300 nm and 7.5 nm min^{-1} from the cross-section SEM as shown in Fig. 2.

3.2. Galvanostatic charge discharge test

Ten charge–discharge cycles were conducted between 3.0 and 4.2 V under 15 μA cm^{-2} constant current before any diffusion measurements were performed. A typical charge–discharge curve is shown in Fig. 3. The incremental capacity ($\Delta Q/\Delta V$) versus potential is shown in Fig. 4. The major peak at about 3.9 V, corresponding to the large plateau in the charge–discharge curve, is due to a first-order phase transition between two different hexagonal phases driven by the metal–insulator transition [1]. Two minor peaks above 4.0 V, corresponding to the two small plateaus in the charge–discharge curve, are due to the two-phase regions on both sides of the ordered $Li_{0.5}CoO_2$ phase [16]. The difference between peak positions during deintercalation and intercalation of Li is about 30 mV, which indicates a small amount of polarization in this cell. The ordered phase

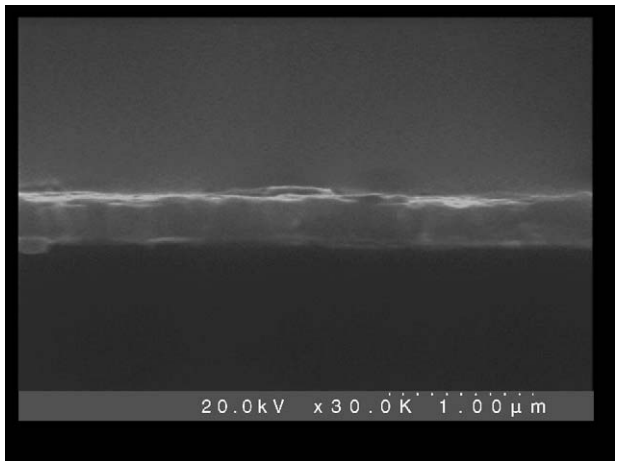

Fig. 2. Cross-sectional SEM image of a $LiCoO_2$ thin film on a Pt/Ti/SiO_2/Si substrate.

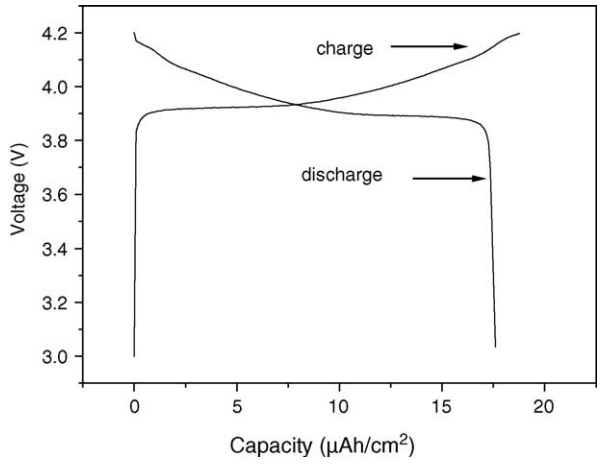

Fig. 3. A typical charge–discharge curve of $LiCoO_2$ thin film grown by PLD.

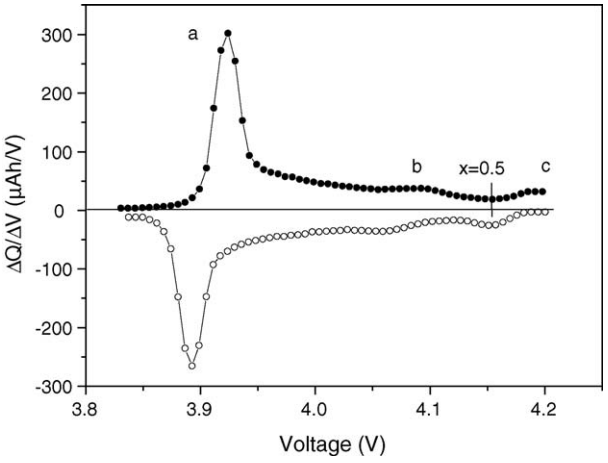

Fig. 4. Incremental capacities ($\Delta Q/\Delta V$) vs. potential derived from charge–discharge curves.

composition $Li_{0.5}CoO_2$ is expected to fall close to the minimum in $\Delta Q/\Delta V$ at 4.15 V [16]. Setting $x = 1/2$ at $V = 4.15$ V allows to derive the potential $V(x)$ in Li_xCoO_2 (Fig. 5) and the derivative $-\mathrm{d}x/\mathrm{d}V$ (Fig. 6).

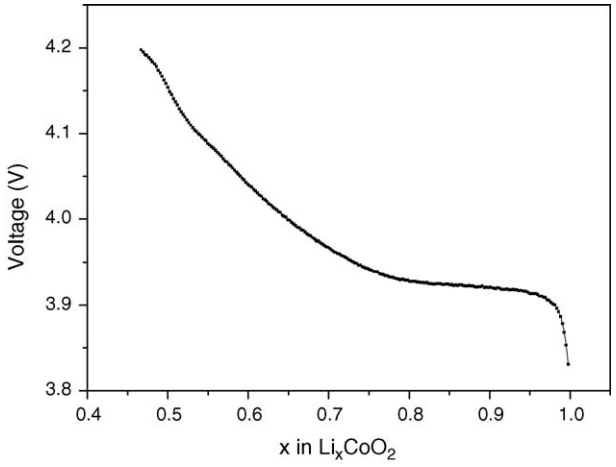

Fig. 5. Coulombic titration curve of a Li_xCoO_2 thin film grown by PLD.

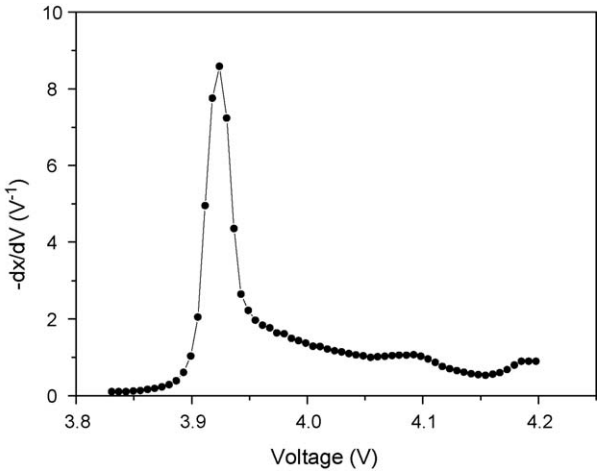

Fig. 6. The derivative $-\mathrm{d}x/\mathrm{d}V$ as a function of cell potential.

3.3. Electrochemical impedance spectroscopy (EIS)

Fig. 7 shows the ac impedance spectra measured in the range of potentials from 3.94 to 4.22 V in 40 mV intervals at open-circuit voltage (OCV) conditions. Before each EIS measurement, the voltage of the cell was kept at a constant value until the current decayed to a stable small value (below 0.1 $\mu A\,cm^{-2}$). Each spectrum behaved similar to the simulated impedance of a Randle's equivalent circuit (Fig. 8). Here, R_o is meant to represent the uncompensated ohmic resistance of the electrolyte and electrode, R_{ct} the charge-transfer resistance, C_{dl} the double layer capacitance of the electrode–electrolyte interface and Z^*_W the complex impedance arising from the diffusion of the electroactive species, which is often referred to the Warburg impedance. The semicircle at high frequencies in the impedance spectrum is due to the parallel combination of C_{dl} and R_{ct}. At low frequencies, a transition occurs when the kinetics pass from charge transfer control to diffusion control, which correspond to a straight line of 45° slope in the spectrum. At very low frequencies, a vertical line emerges in the spectrum due to the onset of finite length diffusion, when R reaches its limiting value given by the sum of $(R_o + R_{ct})$ and R_L. R_L is the limiting low frequency resistance.

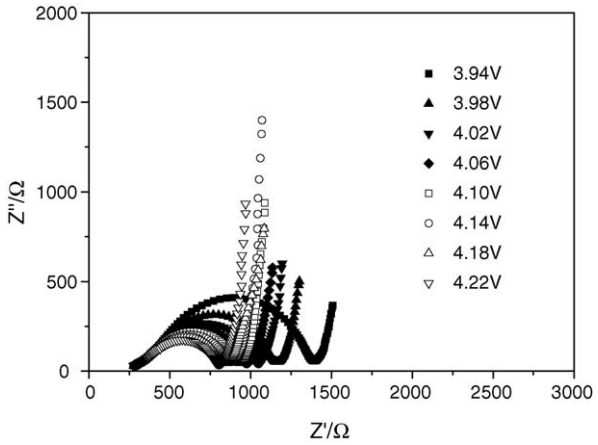

Fig. 7. Cole–Cole plots for $LiCoO_2$ thin films obtained at various potentials.

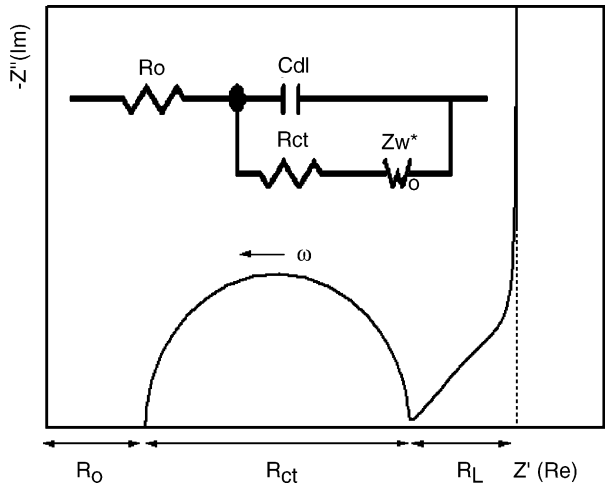

Fig. 8. Simulation of complex impedance using the Randles equivalent circuit.

In case of semi-infinite diffusion, the Warburg impedance Z^*_W can be expressed in terms of an imaginary (X) and real (R) part [17]:

$$Z^*_W = R_W - jX_W \quad (1)$$

with $R_W = |Z| \cos\beta$, $X_W = |Z| \sin\beta$, and $|Z| = |v_o/i_o a|$, and β is the phase of the current with respect to the applied voltage, i_o the amplitude of current density, v_o the amplitude of applied voltage and α the surface area. By solving Fick's second law with proper initial and boundary conditions, the expression of i_o can be deduced as a function of v_o and $\tilde{D}$. A limiting case occurs at very low frequencies when the kinetic pass from semi-infinite diffusion to finite diffusion. The current is 90° out of phase with the voltage and R reaches its limiting value given by the sum of $(R_o + R_{ct})$ and R_L. Under this condition,

$$R_W = R_L = |Z| \cos\beta = \left| \frac{V_M}{zFa} \left(\frac{dV}{dx} \right) \left(\frac{L}{3\tilde{D}} \right) \right| \quad (2)$$

where R_L is the limiting low frequency resistance, which can be obtained by fitting the ac impedance spectra using a equivalent circuit, V_M a molar volume of the $LiCoO_2$ (19.56 $cm^3\ mol^{-1}$), dV/dx can be obtained from $-dx/dV$ in Fig. 6, z is a charge-transfer number of lithium, F the Faraday constant, L the thin film thickness and α the active surface area of the electrode. Therefore, the chemical diffusion coefficient of Li can be calculated from Eq. (2). Fig. 9 shows the chemical diffusion coefficients of Li calculated from Eq. (2) at different potentials. EIS can only be used to obtain the chemical diffusion coefficient in a single-phase region and it is not meaningful to obtain the chemical diffusion coefficient in the two-phase region of $LiCoO_2$ around 3.92 V. The values of $\tilde{D}_{Li}$ range from 3.15×10^{-12} to 1.47×10^{-11} $cm^2\ s^{-1}$ in the voltage range from 3.94 to 4.18 V, which are consistent with previous reports [18]. However, a dip between 4.05 and 4.10 V was found in Fig. 9, which means that $\tilde{D}_{Li}$ does not increase monotonically from 3.94 to 4.18 V.

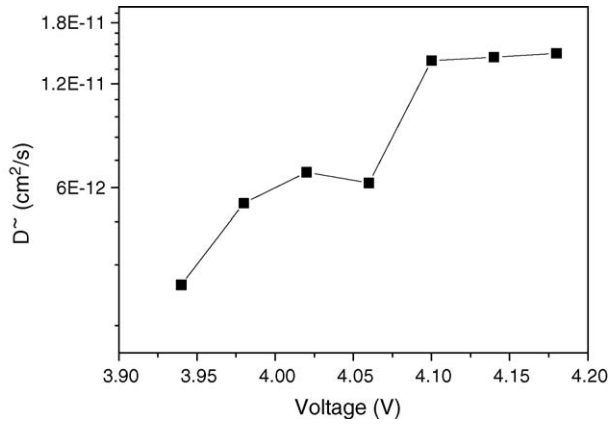

Fig. 9. Chemical diffusion coefficients of Li in a $LiCoO_2$ thin film at various potentials (EIS).

3.4. Potentiostatic intermittent titration technique

In the composition range of $0.46 < x < 0.75$ (from 3.94 to 4.20 V), where Li_xCoO_2 exists in a single-phase region, the current during each potential step decayed exponentially with time. In the composition range of $0.75 < x < 0.93$ (from 3.91 to 3.94 V), where Li_xCoO_2 exists in a two-phase region, the current decay showed a multi-exp behavior [10]. Figs. 10 and 11 show the time dependence of the current of the cell when the potential was decreased from 3.98 to 3.97 V and from 3.97 to 3.96 V, respectively. The semi-logarithmic plots on the inserts in Figs. 10 and 11 show a linear relationship between logarithm of current (ln(I)) and time (t). This allows one to treat the Li diffusion by solving Fick's law for a semi-infinite system with a perturbation of the surface concentration. After the initial transients, the surface current decays exponentially in this diffusion solution [19].

$$I(t) = \frac{2Fa(C_S - C_0)\tilde{D}}{L} \exp\left(-\frac{\pi^2 \tilde{D} t}{4L^2} \right). \quad (3)$$

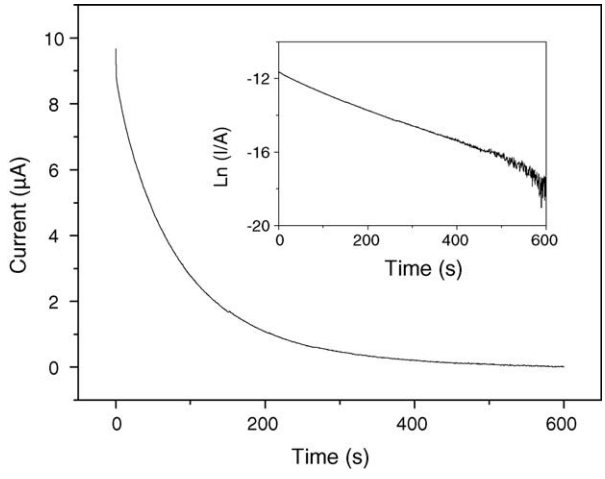

Fig. 10. Time dependence of the current when the potential was decreased from 3.98 to 3.97 V.

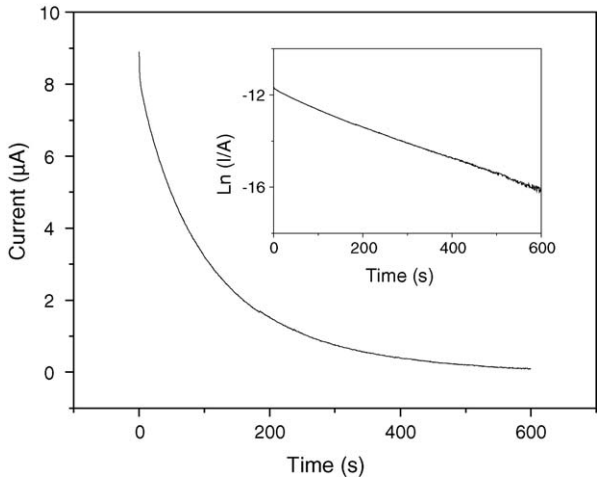

Fig. 11. Time dependence of the current when the potential was decreased from 3.97 to 3.96 V.

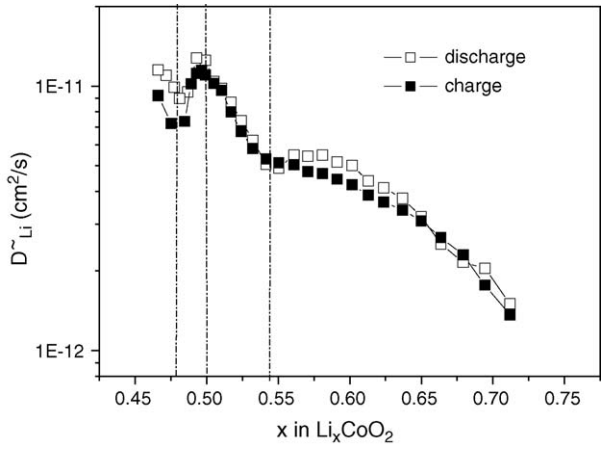

Fig. 13. Chemical diffusion coefficients of Li vs. x in Li_xCoO_2 during charge and discharge states as obtained with PITT.

Therefore, $\tilde{D}$ can be calculated from the slope of the linear region in the plot of ln $I(t)$ versus t.

$$\tilde{D} = -\frac{\mathrm{d}\ \ln(I)}{\mathrm{d}t}\frac{4L^2}{\pi^2} \quad (4)$$

The chemical diffusion coefficients obtained from PITT are plotted as a function of electrode potential during both charge–discharge states in Fig. 12. The values of $\tilde{D}_{Li}$ range from 1.19×10^{-13} to 1.27×10^{-11} $cm^2\ s^{-1}$ in the voltage range from 3.89 to 4.20 V. The values of $\tilde{D}_{Li}$ in $LiCoO_2$ thin films in the literature vary from 10^{-14} to 10^{-7} $cm^2\ s^{-1}$ [10,18,20–23]. The large difference is mostly attributed to two reasons. One is due to different assumptions of the geometrical factors, such as diffusion length and cross-sectional surface area, used in the calculation of $\tilde{D}$. The other one is due to different orientations of thin films with respect to the substrate. For the highly (0 0 3)-textured $LiCoO_2$ thin films, the Li layers lie parallel to the substrate and perpendicular to the direction of diffusion, which would impede Li diffusion. For (1 1 0) or (1 0 1)–(1 0 4) textured $LiCoO_2$ thin films, the Li layers are aligned vertically or tilted with an angle to the substrate, which would facilitate the Li diffusion.

We find that the chemical diffusion coefficient does not increase monotonically as the potential increases from 3.94 to 4.20 V ($0.46 < x < 0.75$), which is similar to Jang et al.'s results [10] but is different from previous measurements using a liquid electrolyte [18,20–23]. Note that the plot of $\tilde{D}_{Li}$ versus potential shows two minima at 4.08 and 4.19 V for the Li deintercalation process and at 4.06 and 4.17 V for the Li intercalation process, respectively. These potentials correspond to the two minor peaks b and c in the incremental capacity plot (Fig. 4), which are associated with the order/disorder transitions near the composition $Li_{0.5}CoO_2$ as mentioned above. In the two-phase region ($0.75 < x < 0.93$), Li transport is due to phase boundary movement. As the phase boundary movement involves two diffusion terms associated with each phase and a boundary kinetic term, it is impossible to calculate $\tilde{D}_{Li}$ as a single value hence the dip in $\tilde{D}_{Li}$ near 3.92 V may not be related. Indeed, Han et al. [24] shows by simulation of PITT data that the fluctuation of $\tilde{D}_{Li}$ in the two-phase regime depend very much on the approximations used to extract $\tilde{D}_{Li}$. Fig. 13 shows the plot of $\tilde{D}_{Li}$ versus x of Li_xCoO_2 ($0.46 < x < 0.72$). The values of $\tilde{D}_{Li}$ range from 1.50×10^{-12} to 1.27×10^{-11} $cm^2\ s^{-1}$ in the single-phase region. Two minima occur at $x = 0.48$ and $x = 0.54$, respectively, and one maximum at $x = 0.5$ is observed in Fig. 13, which is in good agreement with the result of Jang et al. [10].

The chemical diffusion coefficient $\tilde{D}_{Li}$ is a product of the self-diffusion coefficient D_{Li} and the thermodynamic factor Θ [25]. Θ is proportional to $-\mathrm{d}V/\mathrm{d}x$, which will have minima at phase boundaries near the composition $Li_{0.5}CoO_2$ and a maximum at composition $Li_{0.5}CoO_2$. As discussed by Van der Ven and Ceder [26], the self-diffusion coefficient D_{Li} should have a minimum at $x = 0.5$ due to a higher activation energy associated with Li jumps in ordered $Li_{0.5}CoO_2$. Whether $\tilde{D}_{Li}$ is maximal or minimal depends on the balance between the thermodynamic factor and the self-diffusion coefficient. A less-ordered $Li_{0.5}CoO_2$ cathode will exhibit a reduced minimum of D_{Li} compared to a well-

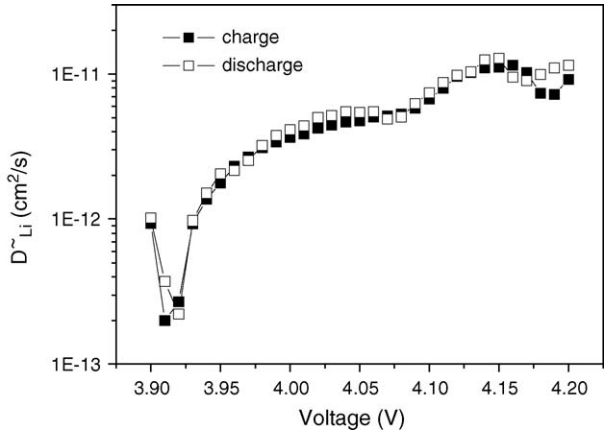

Fig. 12. Chemical diffusion coefficients of Li vs. potential during charge and discharge states (PITT).

ordered $Li_{0.5}CoO_2$ cathode as there would be less limitation to Li jumping. In real experiments, it is difficult to reach the ideal ordered $Li_{0.5}CoO_2$ with a perfect Li vacancy ordering. Therefore, in our case, $\tilde{D}_{Li}$ is mainly determined by the thermodynamic factor Θ, which is why the plot of $\tilde{D}_{Li}$ versus x exhibits characteristics similar to the plot of $-dV/dx$.

3.5. Comparison of EIS and PITT

The chemical diffusion coefficients of Li in the $LiCoO_2$ thin film electrode at different potentials determined by EIS, agree well with the results determined by PITT.

Both techniques are based on the relation between current, voltage and time in a solution to Fick's second law with appropriate initial and boundary conditions. The EIS spectra were measured at a number of different intercalation levels after prolonged potentiostatic equilibration. Therefore, the results obtained from EIS may reflect an equilibrium situation better than the results obtained from PITT. However, the accuracy for calculating the chemical diffusion coefficient of EIS depends on the fitting of the experimental impedance with an equivalent circuit model. Usually there is no good separation between semi-infinite diffusion regime and finite diffusion regime on the experimental impedance spectra so that the fitting may induce some errors when determining the value of R_L, which will directly affect the accuracy for calculating the chemical diffusion coefficient. Although the results of PITT were obtained under a slight deviation from equilibrium conditions, the relationship between the current and time more directly and exactly reflect the diffusion property of Li. Without any fitting, the chemical diffusion coefficient calculated from the relationship between the current and time is more reliable.

4. Conclusions

$LiCoO_2$ thin films with a preferred c-axis orientation were grown on a Si substrate by pulsed laser deposition (PLD). The high quality and dense films without any cracks and pinholes have shown to be excellent test samples for measuring the chemical diffusion coefficient.

The chemical diffusion coefficients of Li in $LiCoO_2$ thin films were investigated by the EIS and PITT methods. The EIS results showed that the chemical diffusion coefficients range from 3.15×10^{-12} to $1.47 \times 10^{-11}\,cm^2\,s^{-1}$ in the potential range from 3.94 to 4.18 V and $\tilde{D}_{Li}$ does not increase monotonically with potential. More detailed results of chemical diffusion coefficients were obtained with PITT, giving values of $\tilde{D}_{Li}$ in the range from $1.\ 50 \times 10^{-12}$ to $1.27 \times 10^{-11}\,cm^2\,s^{-1}$ in the single-phase region of Li_xCoO_2 ($0.46 < x < 0.72$). Two minima at $x = 0.48$ and 0.54 corresponding to order/disorder transitions at phase boundaries near composition $Li_{0.5}CoO_2$ were clearly observed.

Acknowledgements

This research was supported by Advanced Materials for Micro- and Nano-System (AMM&NS) programme under Singapore-MIT Alliance (SMA) and by National University of Singapore. We would like to thank Dr. Y.S. Meng from the Department of Materials Science and Engineering, Massachusetts Institute of Technology, Cambridge and Dr. Songbai Tang from the Department of Mechanical Engineering, National University of Singapore for useful discussions.

References

[1] J. Molenda, A. Stoklosa, T. Bak, Solid State Ion. 36 (1989) 53.
[2] M. Menetrier, I. Saadoune, S. Levasseur, C. Delmas, J. Mater. Chem. 9 (1999) 1135.
[3] C.A. Marianetti, G. Kotliar, G. Ceder, Nat. Mater. 3 (2004) 627.
[4] A. Ven der Ven, M.K. Aydinol, G. Ceder, G. Kresse, J. Hafner, Phys. Rev. B 58 (1998) 2975.
[5] J.N. Reimers, J.R. Dahn, U. von Sacken, J. Electrochem. Soc. 140 (1993) 2752.
[6] A. Honders, J.M. der Kinderen, A.H. van Heeren, J.H.W. de Wit, G.H.J. Broers, Solid State Ion. 15 (1985) 265.
[7] M.G.S.R. Thomas, P.G. Bruce, J.B. Goodenough, Solid State Ion. 17 (1985) 13.
[8] Y.-M. Choi, S.-I. Pyun, J.-S. Bae, S.-I. Moon, J. Power Source 56 (1995) 25.
[9] D. Aurbach, M.D. levi, E. levi, H. Teller, B. Markovsky, G. Salitra, J. Electrochem. Soc. 145 (1998) 3024.
[10] Y.I. Jang, B.J. Neudecker, N.J. Dudney, Electrochem, Solid State Lett. 4 (2001) A74.
[11] K.A. Striebel, C.Z. Deng, S.J. Wen, E.J. Cairns, J. Electrochem. Soc. 143 (1996) 1821.
[12] C. Julien, M.A. Camacho-Lopez, L. Escobar-Alarcon, E. Haro-Poniatowski, Mat. Chem. Phys. 68 (2001) 210.
[13] Y. Iriyama, M. Inaba, T. Abe, Z. Ogumi, J. Power Sources 94 (2001) 175.
[14] J.D. Perkins, C.S. Bahn, J.M. McGraw, P.A. Parilla, D.S. Ginley, J. Electrochem. Soc. 148 (2001) A1302.
[15] J.B. Bates, N.J. Dudney, B.J. Neudecker, F.X. Hart, H.P. Jun, S.A. Hackney, J. Electrochem. Soc. 147 (2000) 59.
[16] J.N. Reimers, J.R. Dahn, U. von Sacken, J. Electrochem. Soc. 140 (1992) 2091.
[17] C. Ho, I.D. Raistrick, R.A. Huggins, J. Electrochem. Soc. 127 (1980) 343.
[18] Y.H. Rho, K. Kanamura, J. Electrochem. Soc. 151 (2004) A1406.
[19] C.J. Wen, B.A. Boukamp, R.A. Huggins, J. Electrochem. Soc. 126 (1979) 2258.
[20] P.J. Bouwman, B.A. Boukamp, H.J.M. Bouwmeester, P.H.L. Notten, J. Electrochem. Soc. 149 (2002) A699.
[21] H. Sato, D. Takahashi, T. Nishina, I. Uchida, J. Power Source 68 (1997) 540.
[22] J.M. McGraw, C.S. Bahn, P.A. Parilla, J.D. Perkins, D.W. Readey, D.S. Ginley, Electrochim. Acta 45 (1999) 187.
[23] M.D. Levi, G. Salitra, B. Markovsky, H. Teller, D. Aurbach, U. Heider, L. Heider, J. Electrochem. Soc. 146 (1999) 1279.
[24] B.C. Han, A. Van der Ven, D. Morgan, G. Ceder, Electrochim. Acta 49 (2004) 4691.
[25] W. Weppner, R.A. Huggins, J. Electrochem. Soc. 124 (1977) 1569.
[26] A. Van der Ven, G. Ceder, Electrochem. Solid State Lett. 3 (2000) 301.